



## Preparation and Enhanced Photocatalytic Hydrogen Evolution Activity of Graphene Based Pd and TiO<sub>2</sub> Composites Synthesized by Chemical Vapour Deposition Method

SHU YUE<sup>1</sup>, DINH CUNG TIEN NGUYEN<sup>2</sup> and WON-CHUN OH<sup>2,\*</sup>

<sup>1</sup>School of Material & Chemical Engineering, Bengbu University, Bengbu 233-030, P.R. China

<sup>2</sup>Department of Advanced Materials Science & Engineering, Hanseo University, Chungnam 356-706, Republic of Korea

\*Corresponding author: Fax:+82 41 6883352; Tel: +82 41 6601337; E-mail: wc\_oh@hanseo.ac.kr

Received: 31 March 2018;

Accepted: 27 June 2018;

Published online: 31 August 2018;

AJC-19040

In this paper, we report a new device for photocatalytic performance with two kinds of graphene. The chemical vapour deposition growth graphene (CVDG) and chemically synthesized graphene were further doped with palladium and titanium dioxide to form the photocatalyst, respectively. The synthesized graphene and as-prepared photocatalysts were characterized by X-ray diffraction, scanning electron microscopy with energy dispersive X-ray (EDX) spectroscopy, TEM (HRTEM) and Raman spectra. From the photocatalytic H<sub>2</sub> evolution effect, it illustrates that the chemical vapour deposition growth graphene based photocatalyst presents better effect than that of chemically synthesized graphene. The present chemical vapour deposition growth graphene based photocatalyst have a potential catalytic conversion of solar energy to clean hydrogen energy under visible light.

**Keywords:** Graphene, H<sub>2</sub> evolution, Chemical vapour deposition, Composites, Raman spectra.

### INTRODUCTION

A two-dimensional allotrope of carbon, namely graphene, is a planar sheet of single-atom thickness. It consists of *sp*<sup>2</sup>-bonded carbon atoms densely packed in a honeycomb crystal lattice. Graphene has awakened considerable scientific interest because of its excellent structural and electrical properties [1], such as high fracture strength (125 GPa) [2], high elasticity (Young's modulus 1100 GPa) [2], high-thermal conductivity (approximately 5000 W m<sup>-1</sup> K<sup>-1</sup>) [3], high mobility of charge carriers (20,000 cm<sup>2</sup> V<sup>-1</sup> s<sup>-1</sup>), [4] and high specific surface area (2630 m<sup>2</sup> g<sup>-1</sup>) [5]. Moreover, graphene has considerable potential for application in electronic and sensing devices owing to its tunable band gap and high electron mobility. The behaviour of charge carriers in graphene is similar to that of Dirac fermions [1], which results in electron mobilities as high as 2 × 10<sup>5</sup> cm<sup>2</sup>/V s [4], ballistic transport over a distance of up to 1 μm at room temperature [6], the half-integer quantum Hall effect [7] and absorption of only 2.3 % of visible light [8]. These properties make graphene a suitable candidate material for use in high-frequency electronics [9], high-performance chemical- and biosensors, transparent conductors, optoelectronics, flexible

flat panel displays [10] and photocatalytic hydrogen evolution [11-15]. The future applications of graphene necessitate the discovery and standardization of methods to synthesize graphene films with large areas and high quality (crystallinity). Chemical synthesis, silicon sublimation from SiC crystals [16-18] and chemical vapour deposition (CVD) using transition metal catalysts [19-22] are some of the methods currently used to synthesize graphene. Chemical vapour deposition is currently the most suitable method for commercial graphene production because it can yield graphene films with large surface areas at a relatively low cost. Chemical vapour deposition using copper is the most promising because this system selectively produces monolayers or multilayers of graphene. The use of other transition metal produces multilayer graphene films with non-uniform thickness, which are unacceptable for use in devices [23-25].

Producing a single-crystalline graphene film through Cu-CVD is currently the main challenge because a graphene film produced through CVD is generally a collage of independently grown, randomly oriented graphene islands [26-29]. Single-crystalline graphene production can be achieved by cautiously controlling carbon atom nucleation and graphene nucleus growth, which depend on CVD process parameters, such as temperature,

pressure and gas flow [30,31]. Herein, we report a novel CVD process for graphene synthesis at a low temperature and atmospheric pressure while benzene was used as the graphene precursor in this process.

Hydrogen energy represents an ideal candidate for supplying the World's future energy needs. It can simultaneously address the energy crisis and environmental pollution caused by the combustion of conventional fossil fuels. Semiconductor-based photocatalytic H<sub>2</sub> evolution from water by using solar irradiation has potential applications in the H<sub>2</sub> economy. Therefore, it has attracted considerable scientific attention [32-36]. Highly efficient visible-light-active semiconductor photocatalysts with narrow band gaps is need to be designed and developed for increasing visible light use. CdS photocatalyst, a type of nanostructured semiconductor, has attracted the maximum attention for water splitting owing to its non-toxicity, high chemical stability and low cost [37,38]. Similarly, TiO<sub>2</sub> is a highly suitable photocatalyst for hydrogen production [39], water purification [40] and air detoxification [41]. Zhang *et al.* [42,43] reported that graphene-incorporated TiO<sub>2</sub> exhibits considerably enhanced the photocatalytic activity of TiO<sub>2</sub>. Mukherji *et al.* [21] reported that nitrogen-doped Sr<sub>2</sub>Ta<sub>2</sub>O<sub>7</sub> exhibits considerably enhanced photocatalytic hydrogen production when coupled with graphene. Furthermore, the deposition of noble metals (Pt, Ag and Pd) on TiO<sub>2</sub> (semiconductor) nanoparticles has been reported to induce a response to visible light and enhance the separation of electron-hole pairs; both these effects can improve the photocatalytic efficiency of TiO<sub>2</sub>.

Herein, we report a new chemical vapour deposition (CVD) process to synthesize graphene by using benzene as graphene precursor at low temperature and atmospheric pressure. The obtained CVD growth graphene and chemically synthesized graphene was further decorated with palladium and titanium dioxide (TiO<sub>2</sub>) to form a photocatalyst, respectively. The photo-

catalytic effect of as-prepared photocatalysts were evaluated by H<sub>2</sub> evolution under visible light irradiation.

## EXPERIMENTAL

**CVD growth and chemical synthesis of graphene:** Graphite was commercially available and purchased from TIMCAL Chemical Co. Ltd., Switzerland. Benzene, a carbon precursor, was purchased from Dae-Jung Chemical and Metals Co. Ltd. Korea. Copper foil (99.9 %), annealed uncoated was used as the substrate for graphene growth. Argon and nitrogen gas were purchased from Samchun Pure Chemical Co. Ltd., Korea. A split Si tube furnace, consisting of an inner and outer tube, was specifically designed for the study. The tube was 30 cm long and had an outer diameter of 4 cm. It had two nozzles. One nozzle was an inlet of benzene vapours, while the other served as the inlet of argon and nitrogen gas. The inner furnace also called the heating zone, (length: 10 cm; diameter: 5 cm) was used to grow graphene on the copper foil. First, benzene vapours were produced by heating it to below its boiling temperature. The vapours were then transferred to the tube simultaneously with argon gas, which served as a carrier for the vapours and prevented the Cu foil reacting with water molecules. The vapour flow and argon gas ratio were controlled through the control valve [44]. The furnace was heated to 500 °C in the first step and argon gas was released into the Si furnace. At about 500 °C, a Cu foil was inserted in the inner tube followed by controlled amount of argon gas and benzene vapours. The growth of graphene was checked at 500 °C after a reaction time of 5 min and the obtained samples was analyzed through high-resolution transmission electron microscopy (HRTEM) and transmission electron microscopy (TEM). Subsequently, graphene (with large surface area) deposited on the Cu foil was isolated by etching [45]; the powder thus obtained was named CVDG powder. Fig. 1 shows the typical process of graphene growth. Chemically, synth-

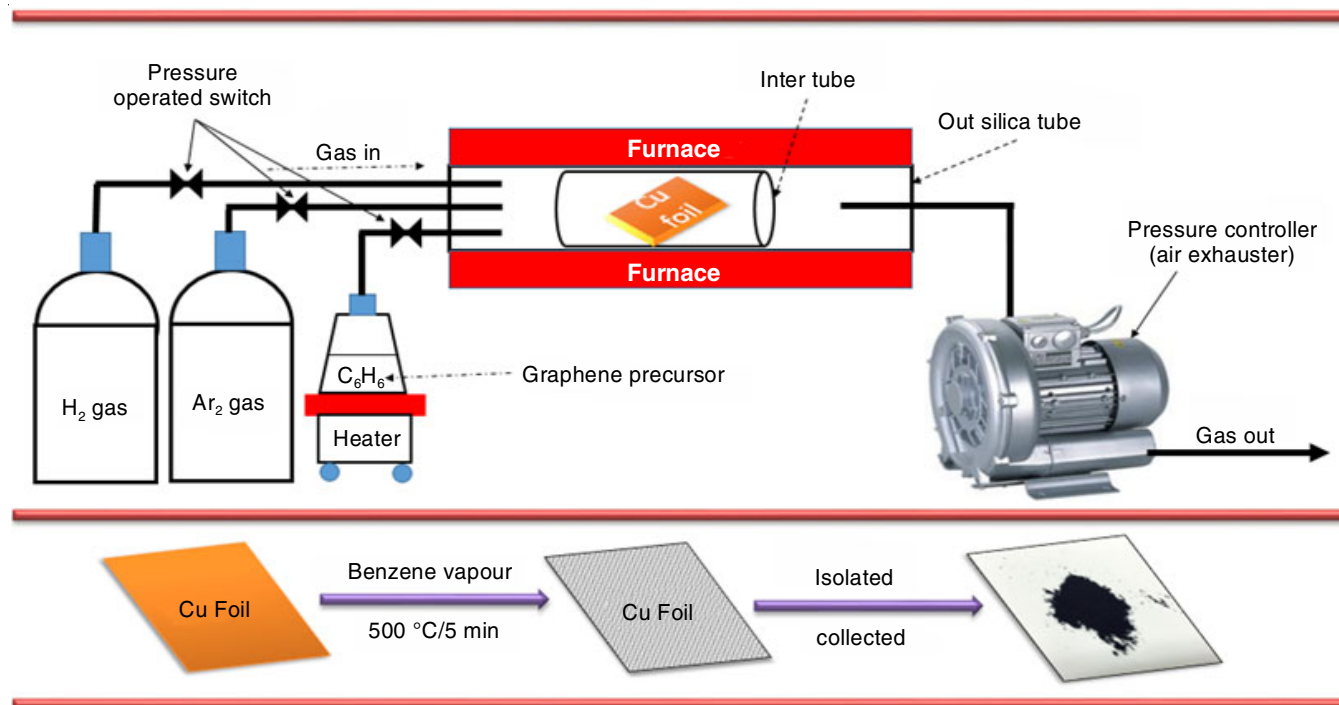


Fig. 1. Schematic of large-area growth on Cu foil by using atmospheric CVD

esized graphene was first mechanically exfoliated from graphite in 2009 [46]. This cost-effective and simple technique has been widely credited for the rapid growth of scientific interest in graphene. The properties of graphene were elucidated after studies on graphene flakes. However, they are usually large (several  $\mu\text{m}$  or tens of  $\mu\text{m}$  in size) and irregularly shaped. Moreover, the azimuthal orientation of the flakes is not deterministically controlled.

**Synthesis of Pd-CVDG/T and Pd-CG/T:** An ethylene glycol solution (20 mL) to which 0.05 mmol  $\text{PdCl}_2$ , 100 mg CVDG powder/G powder and 2 mL TNB were added was stirred vigorously to enable dispersion and form a stable suspension. The suspension was constantly stirred and subjected to ultrasonication by using a 750W, Ultrasonic Processor (VCX 750, Korea) for 4 h. Next, the black solution was filtered, washed three times with deionized water and ethanol, and then dried at 273K. Finally, the sample was heated at 873 K for 1 h. The obtained sample was named Pd-CVDG/T and Pd-CG/T.

**Characterization:** XRD (Shimata XD-D1, Japan) with  $\text{CuK}\alpha$  radiation  $2\theta$  ( $10^\circ$  to  $80^\circ$ ) and a scan speed of 1.20 mL was performed. Elemental analysis was performed using energy dispersive X-ray spectroscopy (EDX). The surface state and structure of graphene growth on Cu foil were observed at an acceleration voltage of 200 kV through HRTEM (JEOL, JEM-2010, Japan). The surface state and structure of photocatalyst composites were observed through TEM (JEOL, JEM-2010, Japan). TEM was also used to examine the size and distribution of palladium particles deposited on the graphene sheet. Raman analysis revealed the signature of graphene on the metallic substrate. A "labRam Aramis" Horiba Jobin Yvon spectrometer equipped with 514 nm argon-ion laser was used for the measurement. The measurements were performed using back scattering geometry. The size of Raman excitation beam spot was approximately 1  $\mu\text{m}$  in diameter.

**Hydrogen evolution performance:** The photocatalytic reaction was carried out at room temperature. The photocatalyst powder 50 mg as-prepared samples were dispersed by magnetic stirrer in 150 mL aqueous solution containing  $0.1 \text{ mol L}^{-1} \text{Na}_2\text{S}$  and  $0.04 \text{ mol L}^{-1} \text{Na}_2\text{SO}_3$  and 20 % methanol as a sacrificial reagent. Visible light source (5 W) was used at a distance of 20 cm from the glass reactor. The amount of hydrogen gas evolved was detected by Minimax (X13010683) XP  $\text{H}_2$  sensor.

## RESULTS AND DISCUSSION

**Morphological formation and growth of graphene:** The FESEM images of prepared CVD-grown graphene are shown in Fig. 2(a-d). The graphene sample clearly exhibited expected graphene morphology. The graphene sheets were mainly multilayers that were separated by pores formed on the Cu substrate. These pores provided supporting reaction spaces for the attachment of nanoparticles for device applications. From Fig. 2(a-d), no spots or mounds were observed on the surface of graphene. Thus, a reaction time of 5 min is adequate for the growth of a graphene layer on a copper surface at 500  $^\circ\text{C}$ .

The identity of graphene as well as the number of layers formed was confirmed using the TEM image of graphene sample shown in Fig. 3(a-d). Fig. 3(a-b) show that smooth graphene with a large area and mainly three layers was produced. The dark

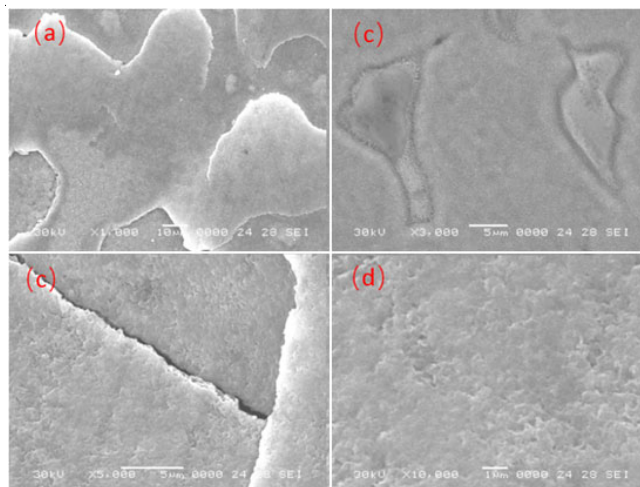


Fig. 2. FESEM images of as prepared graphene (a)  $\times 1000$ ; (b)  $\times 3000$ ; (c)  $\times 5000$ ; (d)  $\times 10000$

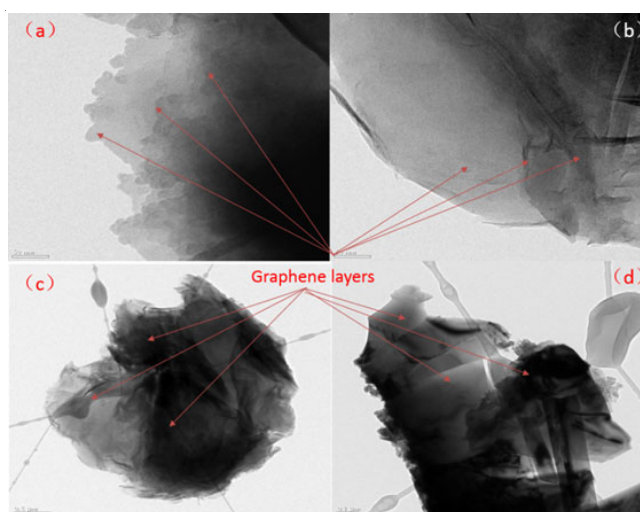


Fig. 3. TEM images of graphene sample (a) 20 nm (b) 20 nm (c) 50 nm (d) 50 nm

region indicated stacked or mainly multilayer graphene with the presence of some wrinkles. These wrinkles may have resulted from the differences between the thermal coefficients of graphene and Cu film [21,26,27]. Moreover, the flow rate of hydrogen and reaction time affect the uniformity, number of layers and degree of defects [47]. Fig. 3(c-d) show high-quality multilayer graphene. Additionally, present results confirmed that benzene vapours and CVD at relatively low temperature (500  $^\circ\text{C}$ ) and normal pressure can be used to produce multilayer graphene. Fig. 4 shows the HRTEM images of an as-prepared sample. The two-dimensional structure of graphene sheet was clearly retained with partial agglomeration in Fig. 4(a-b). Multilayer graphene structure was clear (Fig. 4c-d). The HRTEM images further confirmed that present sample was that of multilayer graphene.

**Characterization of Pd-CVDG/T and Pd-CG/T samples:**

Fig. 5 shows the XRD patterns for  $\text{TiO}_2$ , Pd-CVDG/T and Pd-CG/T samples. The (002) diffraction peak of graphene shifted to a relatively high angle ( $2\theta = 26.2^\circ$ ). The XRD patterns of Pd-CVDG/T and Pd-CG/T nanocomposites revealed strong diffraction peaks at the angles  $39.7^\circ$ ,  $46.0^\circ$ ,  $67.4^\circ$ ,  $80.1^\circ$  and

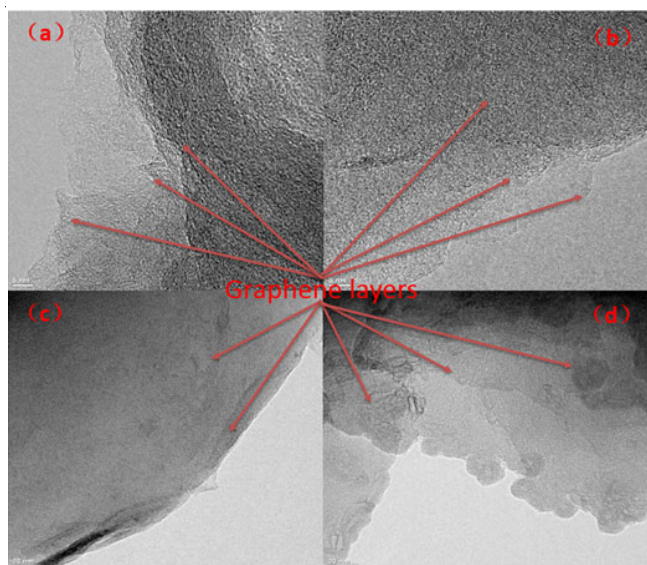


Fig. 4. HRTEM images of graphene sample (a) 20 nm (b) 20 nm (c) 50 nm (d) 50 nm

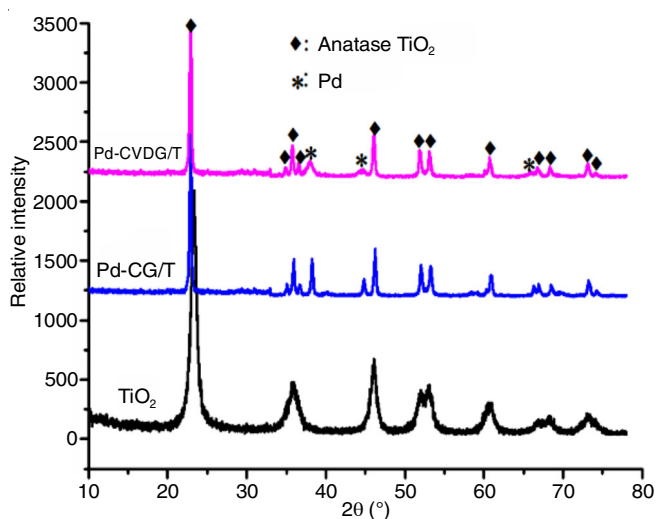


Fig. 5. XRD pattern of TiO<sub>2</sub>, Pd-CVDG/T and Pd-CG/T samples

85°, which matched the (111), (200) and (220) as well as (311) and (222) crystal planes of pure palladium with face-centered-cubic phase (JCPDS 65-2868) (48 and 20). The position of the 002 diffraction peak at 26.2° in the XRD indicated that CVDG was further converted to the crystalline graphene and that the conjugated graphene network (*sp*<sup>2</sup> carbon) was re-established [21,22]. This finding also confirmed that the structures of CVDG and graphene were not adversely affected by the ultrasonic process.

The numerical results of EDX quantitative microanalysis are listed in Table-1. In the entire spectrum, the carbon elemental peak originated from the CVDG and chemically synthesized graphene sheet. The peaks of Ti and O arose from the TiO<sub>2</sub> precursor material, while the peak of Pd element resulted from the presence of PdCl<sub>2</sub>.

The TEM images of each sample were recorded to aid nano-scale structural investigation (Fig. 6). The Pd particles were attached closely to the TiO<sub>2</sub> surface; hence, they appeared relatively dark (Fig. 6b-c). The Pd particles were relatively small and unevenly distributed on CVDG and chemically synthesized graphene sheets. The Pd particles appeared as highly agglomerated particles, which formed clusters of composites. Therefore, the presence of Pd particles resulted in a dark, almost blackened image. The TiO<sub>2</sub> particles were spherical structures larger than the Pd particles and showed a relatively light image. Thus, the TEM imaging of Pd-CVDG/T and Pd-G/T composites provided acceptable information to enable identification. From Fig. 6b-c, the CVDG sheets size was about 50 nm, which was larger than graphene (30 nm). All the dispersion state of these two samples was extremely high.

Fig. 7 describes the Raman spectra of Pd-CVDG/T and Pd-CG/T samples. The variation in Raman band intensity and shift provided information on the nature of C-C bonds and defects. The Raman spectra showed characteristic D and G bands at 1354 and 1590 cm<sup>-1</sup> observed in CVDG and chemically synthesized graphene, respectively (Fig.7). In carbon, *sp*<sup>3</sup> defects are commonly indicated by the D band, while the G band provides information regarding in-plane vibrations of *sp*<sup>2</sup> bonded carbons

TABLE-1  
ENERGY DISPERSIVE X-RAY ELEMENTAL MICROANALYSIS (wt %) OF TiO<sub>2</sub>, Pd-CVDG/T AND Pd-CG/T SAMPLES

Sample	Element				Impurity	Total
	C	O	Pd	Ti		
TiO <sub>2</sub>	0.00	45.22	0.00	54.36	0.42	100.00
Pd-CG/T	49.45	24.34	4.74	21.15	0.32	100.00
Pd-CVDG/T	49.47	24.19	4.73	21.03	0.58	100.00

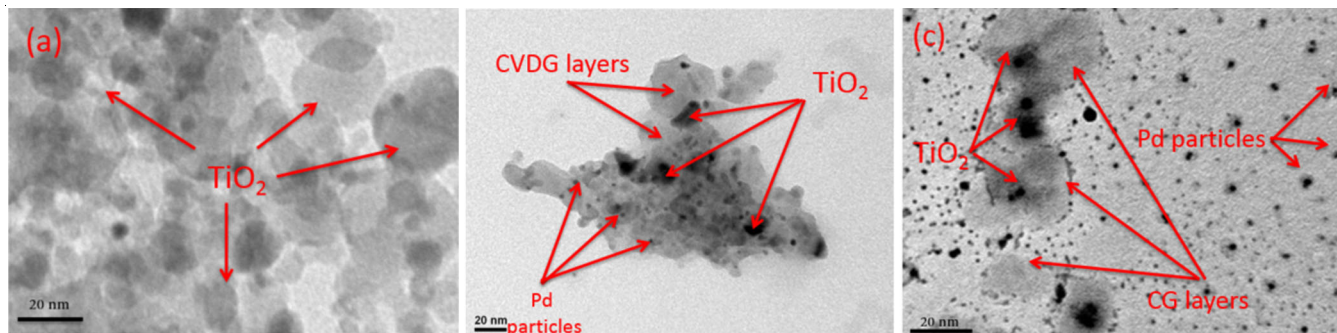


Fig. 6. TEM images of (a) TiO<sub>2</sub>; (b) Pd-CVDG/T; (c) Pd-CG/T sample

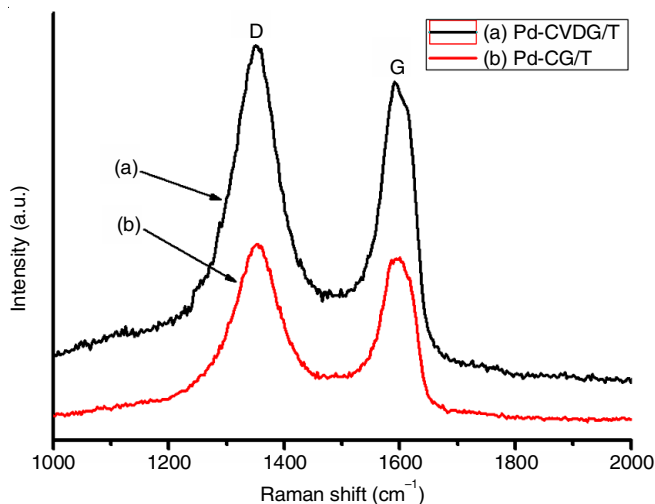


Fig. 7. Raman spectra of (a) Pd-CVDG/T and (b) Pd-CG/T composites

[23-25]. The Pd-CVDG/T and Pd-CG/T nanocomposites exhibited D and G bands, which confirmed the presence of graphene. Furthermore, the calculated values of ID/IG of these two samples were lower than the value of graphene oxide (GO), thus indicating a relatively low density of defects present in Pd-CVDG/T and Pd-CG/T samples. Therefore, the presence of graphene in both the as-prepared samples was indicated by the differences in the Raman band intensity and the blue shift of G band.

#### Mechanism of chemical vapour deposition of graphene:

In metals, such as copper, which have a low carbon solubility, carbon atoms nucleate and laterally expand around the nucleus to form graphene domains when hydrocarbon substrates decompose at high temperatures in catalyzed reaction. The growth stops when the substrate is completely covered by the graphene layer. This process is known as the "self-limited surface deposition" growth mechanism (Fig. 8a). Recently, methods to stop the self-limiting growth process on copper have been reported. Consequently, graphene with relatively few layers can be produced under special growth conditions, such as CVD growth under atmospheric pressure [12,18,19], a low cooling rate [34] and a high methane concentration [35].

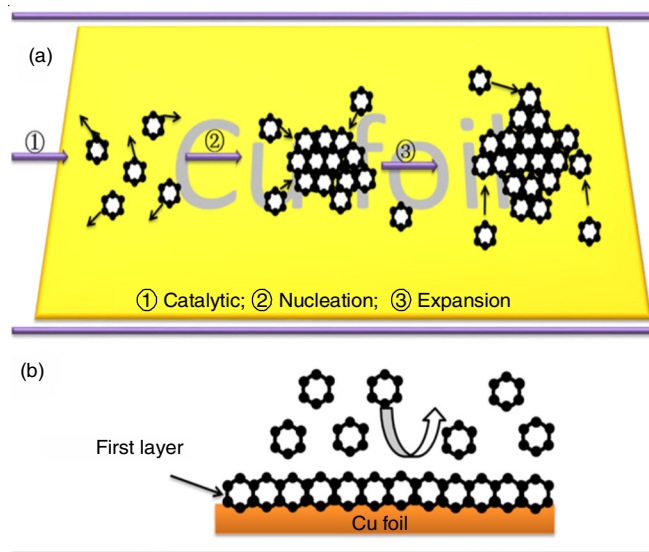


Fig. 8. Schematics diagram of CVD graphene grown on Cu foil

Although carbon exhibits a low solubility in copper, several studies have reported the occurrence of a segregation growth process on Cu enclosures, where carbon species penetrate the Cu foil and forms a second layer or multilayer graphene underneath the first layer on the top [36-38]. This mechanism is known as the "penetration" growth mode (Fig. 8b) [39,49,50], which favor the production of large-scale bilayer or multilayer graphene.

**Photochemical hydrogen production:** The as-prepared Pd-CVDG/T and Pd-CG/T nanocomposites (0.05 g) were dispersed suitably in 100 mL of an aqueous solution containing  $\text{Na}_2\text{S}/\text{Na}_2\text{SO}_3$  as a sacrificial reagent, respectively. A 356 nm light source was adjusted to expose the maximum area of the sealed container. The quantum yield (QY) was determined using the following equation:

$$np = t \times S \times Q \quad (1)$$

$$\text{QY} (\%) = \frac{n\text{H}}{np} \times 100 \quad (2)$$

where,  $np$  is the amount of incident photons,  $t$  is irradiation time,  $s$  is irradiation area in  $\text{m}^2$  and  $Q$  is photon flux of incident light. The quantum yield (QY) (%) was calculated using the ratio of the number of reacted electrons during hydrogen evolution to the number of incident photons according to eqn. 2, where  $n\text{H}$  is the amount of photogenerated  $\text{H}_2$  [21,26]. The photocatalytic  $\text{H}_2$  evolution and quantum yield efficiency (QYs) for the as-prepared samples after 2 h irradiation are shown in Figs. 9 and 10, respectively. The quantum yield efficiency (QYs) of individual Pd-CVDG/T and Pd-CG/T nanocomposite were 4.2 and 3.3 % respectively, using  $\text{Na}_2\text{S}/\text{Na}_2\text{SO}_3$  as the reagent.

The  $\text{H}_2$  evolution and quantum yield (QY) efficiency recorded for  $\text{TiO}_2$  were smaller than those recorded for Pd-CVDG/T and Pd-CG/T nanocomposite under identical conditions. The decrease in  $\text{H}_2$  evolution and corresponding QY efficiency may have been attributed to the fast recombination rate of the excited electrons-hole pair in  $\text{TiO}_2$ . These results highlight the importance of synergistic effect between Pd and the CVDG or G layers, which is absent in  $\text{TiO}_2$ . The Pd-CVDG/T sample exhibited a higher QY efficiency than did the Pd-CG/T sample under identical conditions. This difference may be attributable to the difference in the sizes of graphene layers. The sacrificial reagent provided

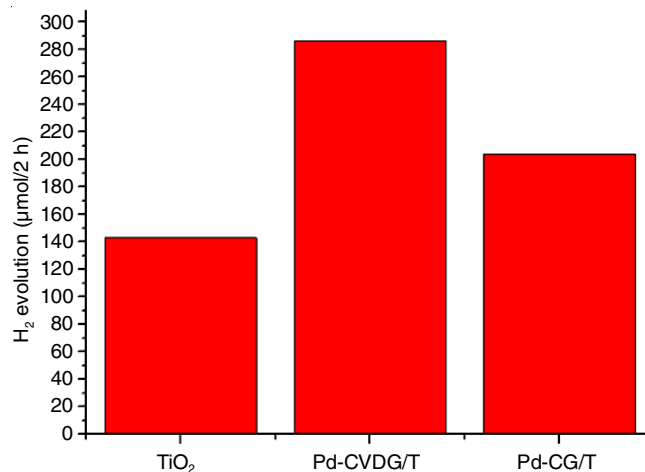


Fig. 9. Photocatalytic  $\text{H}_2$  evolution of  $\text{TiO}_2$ , Pd-CVDG/T and Pd-CG/T samples using  $\text{Na}_2\text{S}/\text{Na}_2\text{SO}_3$  as the sacrificial reagent

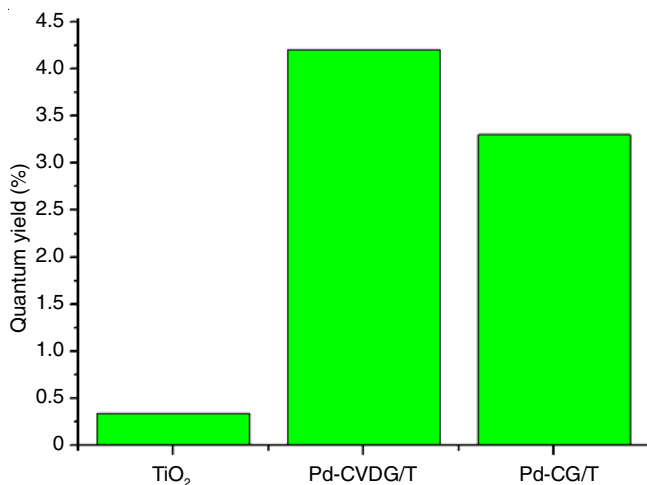


Fig. 10. Photocatalytic H<sub>2</sub> evolution by TiO<sub>2</sub>, Pd-CVDG/T and Pd-CG/T samples with Na<sub>2</sub>S/Na<sub>2</sub>SO<sub>3</sub>

electrons for combination with the photogenerated holes, while TiO<sub>2</sub> served as a reaction center for the production of H<sub>2</sub> from water. The H<sub>2</sub> evolution plots for 20 % methanol solutions with TiO<sub>2</sub>, Pd-CVDG/T and Pd-CG/T as photocatalysts are shown in Fig. 11, Pd-CVDG/T also showed higher effect than Pd-CG/T.

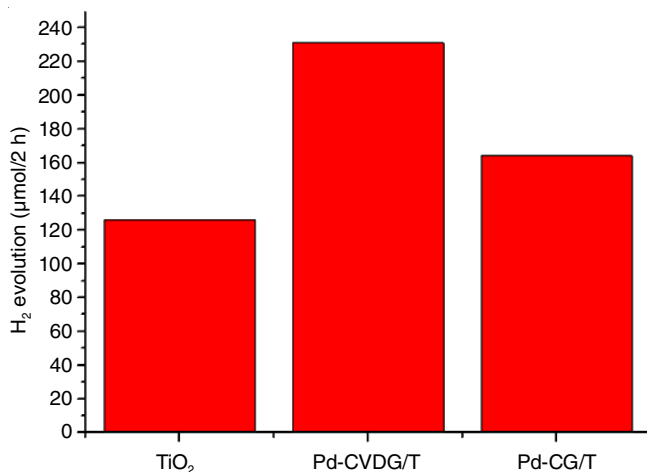


Fig. 11. Photocatalytic H<sub>2</sub> evolution of TiO<sub>2</sub>, Pd-CVDG/T and Pd-CG/T samples using 20 % methanol as the sacrificial reagent

The photostability and cyclic performance of Pd-CVDG/T composite photocatalysts were demonstrated by conducting cyclic photocatalytic H<sub>2</sub> evolution experiments. The photocatalysts exhibited a minor loss in photocatalytic activity for H<sub>2</sub> evolution under identical conditions after five runs, thus indicating the photocatalytic stability of present nanocomposite (Fig. 12). The quantum yield efficiency of reused catalyst did not change notably; hence, the nanocomposite catalysts exhibited excellent chemical stability, which is a highly beneficial characteristic for practical applications. The possible reasons supporting H<sub>2</sub> evolution by using the composite catalyst in visible light are as following. First, the photocatalytic activity of Pd-CVDG/T composite catalyst might be attributable to light absorption in the visible region owing to palladium and CVDG incorporation. Second, in Pd-CVDG/T system, excited electrons from TiO<sub>2</sub> could have been transferred from the

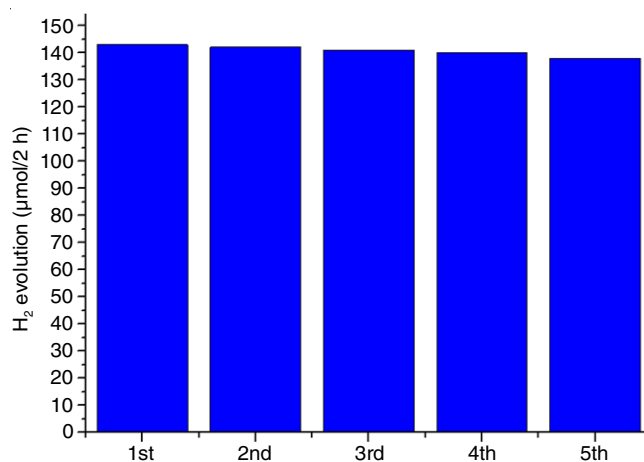


Fig. 12. Cyclic test of the Pd-CVDG/T nanocomposite using Na<sub>2</sub>S/Na<sub>2</sub>SO<sub>3</sub> as the sacrificial reagent

conduction band to CVDG through the mechanism of percolation [32]. Thus in the composite, CVDG acted as an acceptor of TiO<sub>2</sub>-generated electrons; hence, it effectively suppressed the recombination of charge. Consequently, a high number of charge carriers were available to form reactive species and promote the H<sub>2</sub> evolution [11,33].

## Conclusion

In conclusion, we proposed and investigated a new and short method for producing large-area graphene films. This large-area graphene films can be generated through large-scale production in industries by optimizing experimental parameters. We demonstrated the production of CVD-grown graphene in a relatively short reaction time in a H<sub>2</sub>/argon environment. The FESEM, TEM and HRTEM images exhibited multilayer graphene growth on copper foil. The produced large-area graphene film was doped using palladium and TiO<sub>2</sub> nanoparticles successfully by using an ultrasonic method. From TEM images, CVD-grown graphene has larger sheets size than chemically synthesized graphene. Pd-CVDG/T sample is a stable efficient photocatalyst for photocatalytic H<sub>2</sub> evolution from water. This high photocatalytic activity might be attributable to the synergistic effect between palladium and CVDG. Pd-CVDG/T was found to be a potential catalyst for conversion of solar energy to clean hydrogen energy under visible light. However, the evolution of H<sub>2</sub> is currently not sufficiently high.

## CONFLICT OF INTEREST

The authors declare that there is no conflict of interests regarding the publication of this article.

## REFERENCES

1. A.C. Ferrari and D.M. Basko, *Nat. Nanotechnol.*, **8**, 235 (2013); <https://doi.org/10.1038/nnano.2013.46>.
2. A. Kasry, M.A. Kuroda, G.J. Martyna, G.S. Tulevski and A.A. Bol, *ACS Nano*, **4**, 3839 (2010); <https://doi.org/10.1021/nn100508g>.
3. A. Reina, X. Jia, J. Ho, D. Nezich, H. Son, V. Bulovic, M.S. Dresselhaus and J. Kong, *Nano Lett.*, **9**, 30 (2009); <https://doi.org/10.1021/nl801827v>.
4. A.A. Balandin, S. Ghosh, W. Bao, I. Calizo, D. Teweldebrhan, F. Miao and C.N. Lau, *Nano Lett.*, **8**, 902 (2008); <https://doi.org/10.1021/nl073187z>.

5. A.C. Ferrari, J.C. Meyer, V. Scardaci, C. Casiraghi, M. Lazzeri, F. Mauri, S. Piscanec, D. Jiang, K.S. Novoselov, S. Roth and A.K. Geim, *Phys Rev Lett.*, **97**, 187401 (2006); <https://doi.org/10.1103/PhysRevLett.97.187401>.
6. A.H. Castro Neto, F. Guinea, N.M.R. Peres, K.S. Novoselov and A.K. Geim, *Rev. Mod. Phys.*, **81**, 109 (2009); <https://doi.org/10.1103/RevModPhys.81.109>.
7. C. Berger, Z. Song, T. Li *et al.*, *Science*, **312**, 1191 (2006); <https://doi.org/10.1126/science.1125925>.
8. C. Lee, X. Wei, J.W. Kysar and J. Hone, *Science*, **321**, 385 (2008); <https://doi.org/10.1126/science.1157996>.
9. C. Tao, L. Jiao, O.V. Yazyev, Y.-C. Chen, J. Feng, X. Zhang, R.B. Capaz, J.M. Tour, A. Zettl, S.G. Louie, H. Dai and M.F. Crommie, *Nat. Phys.*, **7**, 616 (2011); <https://doi.org/10.1038/nphys1991>.
10. C. Kang, D.H. Jung and J.S. Lee, *J. Nanosci. Nanotechnol.*, **15**, 9098 (2015); <https://doi.org/10.1166/jnn.2015.11557>.
11. H. Huang, W. Zhang, Y. Fu and X. Wang, *Electrochim. Acta*, **152**, 480 (2015); <https://doi.org/10.1016/j.electacta.2014.11.162>.
12. H. Wang, G. Wang, P. Bao, S. Yang, W. Zhu, X. Xie and W.-J. Zhang, *J. Am. Chem. Soc.*, **134**, 3627 (2012); <https://doi.org/10.1021/ja2105976>.
13. H. Wang, L.-F. Cui, Y. Yang, H. Sanchez Casalongue, J.T. Robinson, Y. Liang, Y. Cui and H. Dai, *J. Am. Chem. Soc.*, **132**, 13978 (2010); <https://doi.org/10.1021/ja105296a>.
14. J. Aguado, R. Vangrieken, M. Lopezmunoz and J. Marugan, *J. Appl. Catal. A*, **312**, 202 (2006); <https://doi.org/10.1016/j.apcata.2006.07.003>.
15. J. Coraux, A.T. N'Diaye, C. Busse and T. Michely, *Nano Lett.*, **8**, 565 (2008); <https://doi.org/10.1021/nl0728874>.
16. J. Zhao, S. Pei, W. Ren, L. Gao and H.M. Cheng, *ACS Nano*, **4**, 5245 (2010); <https://doi.org/10.1021/nn1015506>.
17. J.K. Wassei and R.B. Kaner, *Mater. Today*, **13**, 52 (2010); [https://doi.org/10.1016/S1369-7021\(10\)70034-1](https://doi.org/10.1016/S1369-7021(10)70034-1).
18. K. Ariyawong, C. Chatillon, E. Blanquet, J.-M. Dedulle and D. Chaussende, *CrystEngComm*, **18**, 2119 (2016); <https://doi.org/10.1039/C5CE02480C>.
19. S.-M. Jeong, D.-H. Nam, B.G. Kim, J.-Y. Yoon, M.-H. Lee, K.-H. Kim, Y.J. Yoon and W.-S. Seo, *Appl. Phys. Expr.*, **7**, 025501 (2014); <https://doi.org/10.7567/APEX.7.025501>.
20. K.A. Ritter and J.W. Lyding, *Nat. Mater.*, **8**, 235 (2009); <https://doi.org/10.1038/nmat2378>.
21. A. Mukherji, B. Seger, G.Q. (Max) Lu and L. Wang, *ACS Nano*, **5**, 3483 (2011); <https://doi.org/10.1021/nn102469e>.
22. K.S. Kim, Y. Zhao, H. Jang, S.Y. Lee, J.M. Kim, K.S. Kim, J.-H. Ahn, P. Kim, J.-Y. Choi and B.H. Hong, *Nature*, **457**, 706 (2009); <https://doi.org/10.1038/nature07719>.
23. K.S. Novoselov, A.K. Geim, S.V. Morozov, D. Jiang, M.I. Katsnelson, I.V. Grigorieva, S.V. Dubonos and A.A. Firsov, *Nature*, **438**, 197 (2005); <https://doi.org/10.1038/nature04233>.
24. K.V. Emtsev, A. Bostwick, K. Horn, J. Jobst, G.L. Kellogg, L. Ley, J.L. McChesney, T. Ohta, S.A. Reshanov, J. Röhrl, E. Rotenberg, A.K. Schmid, D. Waldmann, H.B. Weber and T. Seyller, *Nat. Mater.*, **8**, 203 (2009); <https://doi.org/10.1038/nmat2382>.
25. K. Ullah, S. Ye, L. Zhu, Z.-D. Meng, S. Sarkar and W.-C. Oh, *Mater. Sci. Eng. B*, **180**, 20 (2014); <https://doi.org/10.1016/j.mseb.2013.10.014>.
26. L. Gao, W. Ren, H. Xu, L. Jin, Z. Wang, T. Ma, L.-P. Ma, Z. Zhang, Q. Fu, L.-M. Peng, X. Bao and H.-M. Cheng, *Nat. Commun.*, **3**, 699 (2012); <https://doi.org/10.1038/ncomms1702>.
27. L. Gomez De Arco, Y. Zhang, C.W. Schlenker, K. Ryu, M.E. Thompson and C. Zhou, *ACS Nano*, **4**, 2865 (2010); <https://doi.org/10.1021/nn901587x>.
28. L.M. Malard, M.A. Pimenta, G. Dresselhaus and M.S. Dresselhaus, *Phys. Rep.*, **473**, 51 (2009); <https://doi.org/10.1016/j.physrep.2009.02.003>.
29. L. Gong, I.A. Kinloch, R.J. Young, I. Riaz, R. Jalil and K.S. Novoselov, *Adv. Mater.*, **22**, 2694 (2010); <https://doi.org/10.1002/adma.200904264>.
30. M. Pan, E.C. Girão, X. Jia, S. Bhaviripudi, Q. Li, J. Kong, V. Meunier and M.S. Dresselhaus, *Nano Lett.*, **12**, 1928 (2012); <https://doi.org/10.1021/nl204392s>.
31. M.D. Stoller, S. Park, Y. Zhu, J. An and R.S. Ruoff, *Nano Lett.*, **8**, 3498 (2008); <https://doi.org/10.1021/nl802558y>.
32. P. Ang, W. Chen, A.T.S. Wee and K.P. Loh, *J. Am. Chem. Soc.*, **130**, 14392 (2008); <https://doi.org/10.1021/ja805090z>.
33. P. Sutter, *Nat. Mater.*, **8**, 171 (2009); <https://doi.org/10.1038/nmat2392>.
34. P.W. Sutter, J.I. Flege and E.A. Sutter, *Nat. Mater.*, **7**, 406 (2008); <https://doi.org/10.1038/nmat2166>.
35. P. Maher, L. Wang, Y. Gao, C. Forsythe, T. Taniguchi, K. Watanabe, D. Abanin, Z. Papi, P. Cadden-Zimansky, J. Hone, P. Kim and C.R. Dean, *Science*, **345**, 61 (2014); <https://doi.org/10.1126/science.1252875>.
36. Q. Yu, J. Lian, S. Siriponglert, H. Li, Y.P. Chen and S.-S. Pei, *Appl. Phys. Lett.*, **93**, 113103 (2008); <https://doi.org/10.1063/1.2982585>.
37. R.R. Nair, P. Blake, A.N. Grigorenko, K.S. Novoselov, T.J. Booth, T. Stauber, N.M.R. Peres and A.K. Geim, *Science*, **320**, 1308 (2008); <https://doi.org/10.1126/science.1156965>.
38. S. Hou, M.L. Kasner, S. Su, K. Patel and R. Cuellari, *J. Phys. Chem. C*, **114**, 14915 (2010); <https://doi.org/10.1021/jp1020593>.
39. S. Liu, M.Q. Yang and Y.J. Xu, *J. Mater. Chem. A Mater. Energy Sustain.*, **2**, 430 (2014); <https://doi.org/10.1039/C3TA13892E>.
40. S. Reich and C. Thomsen, *Philos. Trans. R. Soc. Lond. A*, **362**, 2271 (2004); <https://doi.org/10.1098/rsta.2004.1454>.
41. U. Ritter, P. Scharff, C. Siegmund, O.P. Dmytrenko, N.P. Kulish, Y.I. Prylutsky, N.M. Belyi, V.A. Gubanov, L.I. Komarova, S.V. Lizunova, V.G. Poroshin, V.V. Shlapatskaya and H. Bernas, *Carbon*, **44**, 2694 (2006); <https://doi.org/10.1016/j.carbon.2006.04.010>.
42. W. Han, L. Ren, Z. Zhang, X. Qi, Y. Liu, Z. Huang and J. Zhong, *Ceram. Int.*, **41**, 7471 (2015); <https://doi.org/10.1016/j.ceramint.2015.02.068>.
43. Q. Chen, M. Zhou, Z. Zhang, T. Tang and T. Wang, *J. Mater. Sci.: Mater. Electron.*, **28**, 9416 (2017); <https://doi.org/10.1007/s10854-017-6683-2>.
44. X. Du, I. Skachko, A. Barker and E.Y. Andrei, *Nat. Nanotechnol.*, **3**, 491 (2008); <https://doi.org/10.1038/nnano.2008.199>.
45. X. Li, W. Cai, J. An, S. Kim, J. Nah, D. Yang, R. Piner, A. Velamakanni, I. Jung, E. Tutuc, S.K. Banerjee, L. Colombo and R.S. Ruoff, *Science*, **324**, 1312 (2009); <https://doi.org/10.1126/science.1171245>.
46. X. Li, Y. Zhu, W. Cai, M. Borysiak, B. Han, D. Chen, R.D. Piner, L. Colombo and R.S. Ruoff, *Nano Lett.*, **9**, 4359 (2009); <https://doi.org/10.1021/nl902623y>.
47. X. Qi, K. Pu, H. Li, X. Zhou, S. Wu, Q. Fan, B. Liu, F. Boey, W. Huang and H. Zhang, *Angew. Chem. Int. Ed.*, **49**, 9426 (2010); <https://doi.org/10.1002/anie.201004497>.
48. X. Wang, L. Zhi, N. Tsao, Z. Tomovic, J. Li and K. Mullen, *Angew. Chem. Int. Ed.*, **47**, 2990 (2008); <https://doi.org/10.1002/anie.200704909>.
49. X. Zhang, O.V. Yazyev, J. Feng, L. Xie, C. Tao, Y.-C. Chen, L. Jiao, Z. Pedramrazi, A. Zettl, S.G. Louie, H. Dai and M.F. Crommie, *ACS Nano*, **7**, 198 (2013); <https://doi.org/10.1021/nn303730v>.
50. Y.M. Lin, C. Dimitrakopoulos, K.A. Jenkins, D.B. Farmer, H.Y. Chiu, A. Grill and P. Avouris, *Science*, **327**, 662 (2010); <https://doi.org/10.1126/science.1184289>.